Table 2. Up-regulated genes examined for CpG sites in the promoters

Gene	Size of TSS-containing CpG island, bp	Upstream inclusion	No. of satellite CpG islands*	CpG site density†		
				TSS island	Upstream regions	Satellite
AGC	938	Upstream 1 kb	0	H to M	H to M	–
ALPL	815	~350 bp	0	H to M	H to M	–
CHAD	645	~600 bp	0	H	H	–
COL11A2	216	~200 bp	3	H	H	H to M
COL2A1	530	~300 bp	2	H	H	M
COL9A2	902	~350 bp	0	H	H	–
COL9A3	1,207	~700 bp	0	H to M	H to M	–
CPE	729	~70 bp	0	H	–	–
DKK1	498	~300 bp	2	M	M to L	M
FGFR3	2,645	~1.2 kb	0	H	H	–
FMOD	109	Exon 1 only	0	M	L	–
LECT1	1,120	~250 bp	0	H to M	M	–
MATN3	607	~200 bp	0	H	M	–
MATN4	0	–	2	–	L	M
RGS4	160	~50 bp	0	L	L	–
SCUBE3	1,454	~1.1 kb	0	H	H	–
WNT11	711	~400 bp	5	H	H to M	H to M

* Numbers of satellite CpG islands estimated within the 2-kb upstream region.
† Classified according to the percentage of CpG ratios in the island, as high (H), medium (M), or low (L). TSS = transcription start site.

superficial layer, which was defined as a very thin layer of the articular surface measuring <0.5 mm in thickness; the superficial layer, which was defined as the next layer, measuring 1 mm in thickness; the intermediate layer, which was defined as the next layer, measuring ~1.5 mm in thickness; and the deep layer, which was defined as the next layer, measuring ~1 mm in thickness (all roughly estimated).

Purified genomic DNA was subjected to bisulfite conversion using an Epitect DNA bisulfite kit (Qiagen). Converted DNA was PCR amplified using primer sets designed to be within 2 kb upstream of the transcription start sites. Two rounds of amplification were conducted using an AccuPrime *Taq* DNA polymerase system (Invitrogen, Tokyo, Japan) under the following conditions: 95°C for 5 minutes and 30 cycles of 95°C for 1 minute, 52°C for 30 seconds, and 68°C for 30 seconds, followed by 10 minutes' extension at 68°C. PCR products were subcloned into bacteria using a Zero-Blunt cloning kit (Invitrogen), and 6–10 colonies per each condition were sequenced using a BigDye Terminator v1.1 Cycle Sequencing kit and a 31330x Genetic Analyzer (Applied Biosystems, Tokyo, Japan). (The primer sequences used are available online at the authors' Web site: http://www.tmd.ac.jp/mri/mph/kenkyuu00.html.)

RNA isolation and real-time RT-PCR. Total RNA was isolated separately from 3 pellets of human synovium–derived MSCs that had differentiated under chondrogenic conditions for day 21 and from a comparable number of undifferentiated human MSCs (2.4×10^6 cells) before being subjected to chondrogenic conditions (day 0). RNA extraction was performed using TRIzol reagent (Invitrogen). An aliquot of 500 ng of total RNA was subjected to reverse transcription using an RT2 First-Strand kit (SABiosciences, Frederick, MD) according to the manufacturer's instructions. Real-time RT-PCR was performed using SYBR Green Supermix (Bio-Rad, Hercules, CA) and an iCycler-iQ5 detection system (Bio-Rad), followed by quantification. All data were normalized against those of β-actin (*ACTB*) transcripts (27). Specific primers (available online at the authors' Web site: http://www.tmd.ac.jp/mri/mph) were designed using the Primer3 program (28).

Statistical analysis. Statistical analysis was performed with Student's *t*-test to compare the methylation status of promoter regions before and after chondrogenic pellet culture (day 0 and day 21, respectively) as well as for the results of the RT-PCR analysis of the MSCs. The methylation status of the 4 layers of human articular cartilage was compared using one-way analysis of variance. The Tukey-Kramer multiple comparison test was applied as the post hoc test when *P* values derived by the F test were less than 0.05. *P* values less than 0.05 were considered significant.

RESULTS

Analysis of CpG islands in the promoter regions of key transcription factors in chondrogenesis. In order to evaluate the status of CpG island methylation during chondrogenesis, 2 important transcription factors were selected. The *SOX9* upstream sequence had 2 moderate-sized CpG islands (564 bp and 401 bp) within 1.2 kb of the transcription start site, with intermediate CpG site density. The range of CpG-rich sequences and their densities met classic and default definitions of CpG islands according to the MethPrimer program (Figure 1A). Similarly, *RUNX2* had 3 CpG island blocks of sizes 185 bp, 256 bp, and 419 bp within a 1-kb region, with higher CpG density (Figure 1B). Thus, we selected these 2 key transcription factors as candidate targets for regulation through CpG methylation.

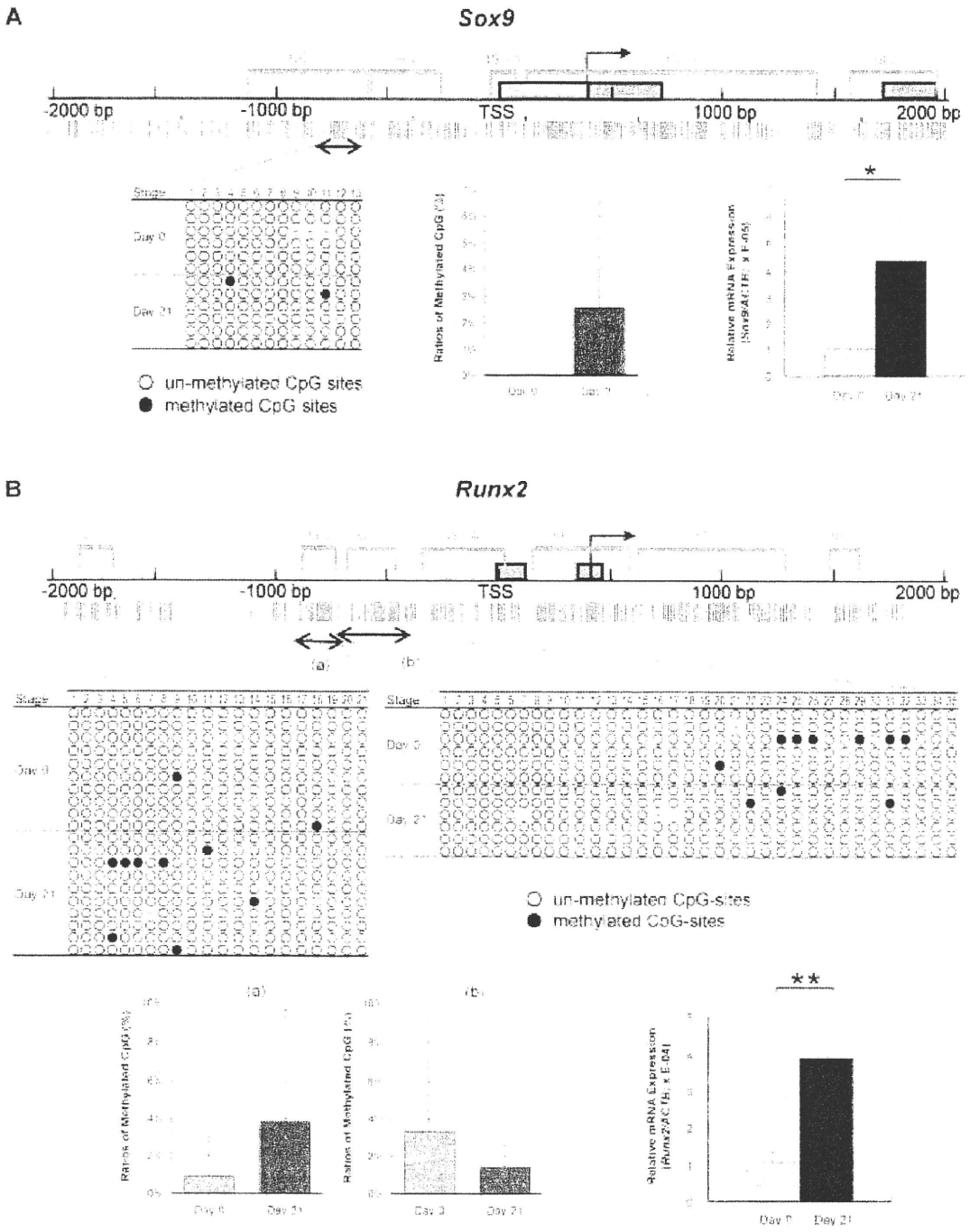

Figure 1. Analysis of CpG islands in key transcription factors involved in chondrogenesis. Structural features of the transcription start site (TSS)–flanking regions (4 kb) of the key transcription factor genes *SOX9* (**A**) and *RUNX2* (**B**) are shown. Structures of exons and introns are indicated by the shaded boxes atop the horizontal line. The scaled horizontal line indicates the genomic DNA sequences, with the transcription start site at zero; scales represent basepairs. The arrow arising from the top of the horizontal line indicates the translation-initiating ATG site. CpG islands (Isl) are indicated by light gray boxes on top of the horizontal line (numbered left to right). Vertical lines beneath the horizontal line indicate the distributions and densities of CpG sites. Double-headed arrows indicate the locations of polymerase chain reaction (PCR) amplicons used in the bisulfite sequencing analysis. Tables show the results of bisulfite sequencing analyses of multiple bacterial colonies (– = methylation status not determined). Bar graphs show the ratio of methylated cytosine in CpG within the regions analyzed, as well as the relative mRNA expression compared with β-actin, as determined by real-time reverse transcription–PCR analysis. Values are the mean and SD of multiple bacterial clones. * = $P < 0.05$; ** = $P < 0.01$, by Student's t-test.

The bisulfite sequencing analysis, however, revealed that no significant methylation was detectable within the analyzed regions of the *SOX9* and *RUNX2* promoters in either the undifferentiated state or the differentiated state induced by 3 weeks of pellet culture (Figure 1). Similar levels of extreme hypomethylation were observed in DNA samples prepared from parallel cultures of human synovium–derived MSCs isolated from independent donors, as well as in the articular cartilage from the knee joint of the OA patient (Figure 2). These data indicate that promoter regions of the key transcription factors *SOX9* and *RUNX2* are hypomethylated regardless of their differentiation status during chondrogenesis.

Analysis of DNA methylation of differentially expressed genes before and after induction of chondrogenesis. We next investigated sequences surrounding transcription start sites of genes whose expression changed remarkably during chondrogenesis. Searching through previous microarray data obtained on similar MSCs that had been subjected to chondrogenic pellet culture (25), we selected 4 up-regulated and 4 down-regulated signature genes for methylation analysis: *CHM1*, *MATN4*, *FGFR3*, and *CHAD* were selected as up-regulated genes, and *SOX4*, *GREM1*, *GPR39*, and *SDF1* were selected as down-regulated genes. For this selection, we chose genes with CpG islands that were closer to the transcription start site and had CpG sites of intermediate density. The promoter region of *MATN4*, which is of low CpG site density (Table 2 and Figure 3D), was included in the study to serve as a reference sequence with low CpG content.

The hypomethylation status of the CpG-rich promoter regions was indicated by bisulfite sequencing in most of these 8 genes: *CHM1*, *FGFR3*, and *CHAD* (Figures 3A–C), as well as *SOX4*, *GREM1*, and *GPR39* (Figures 4A–C), and this hypomethylation status was unchanged before and after induction of chondrogenesis. The levels of hypomethylation were similar between culture samples within the same experimental groups and in the articular cartilage from the patient with OA (Figure 2). In contrast, we observed high levels of methylation in the promoter sequence of *MATN4*, which was tested as a positive control (Figure 3D). This hypermethylation status was maintained even after induction of chondrogenesis, which induced *MATN4* expression. This finding is consistent with the notion that genomic DNA regions with a low density of CpG sites tend to be hypermethylated, presumably having little effect on the activation status for transcription in many cases (7,8). Thus, our observations about methylation status during chondrogenesis were consistent overall, because similar levels of CpG hypomethylation were

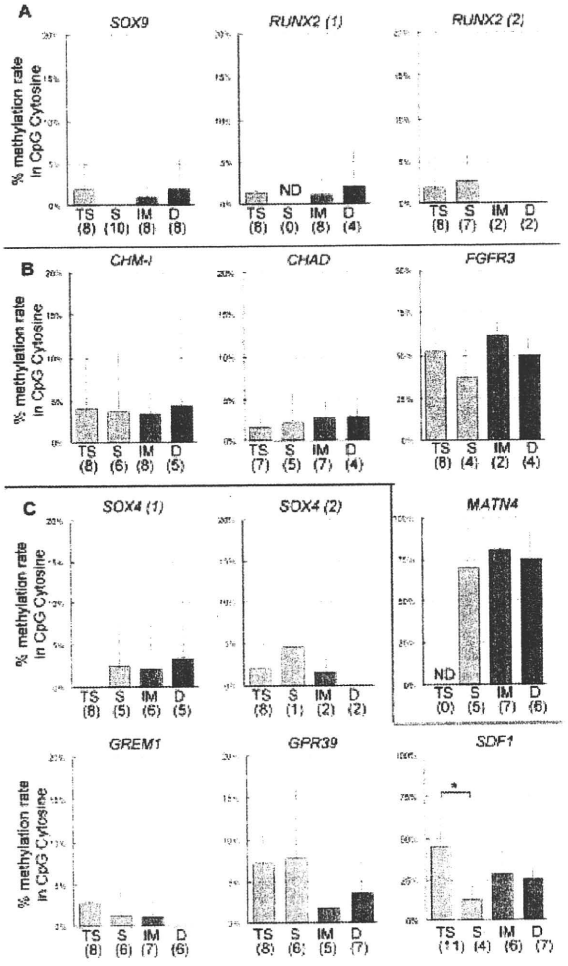

Figure 2. Bisulfite sequence analysis of the signature genes in articular cartilage from a patient with osteoarthritis. The methylation status of 12 genomic regions of 10 genes was analyzed in 4 cartilage layers: tangential superficial (TS), superficial (S), intermediate (IM), and deep (D) layers. Bisulfite sequencing was used to determine the methylation status of **A**, genes encoding transcription factors important for chondrocyte lineage commitment (*SOX9* and *RUNX2* [2 regions of interest, corresponding to a and b in Figure 1B]), **B**, genes up-regulated in chondrogenic pellet cultures (*CHM1*, *CHAD*, *FGFR3*, and *MATN4*), and **C**, genes down-regulated in chondrogenic pellet cultures (*SOX4* [2 regions of interest, corresponding to a and b in Figure 4A], *GREM1*, *GPR39*, and *SDF1*). The methylation rate (%) for the CpG sites in each region was calculated for each cartilage layer. Values are the mean and SD. Numbers in parentheses are the number of bacterial clones analyzed. * = $P < 0.01$ by one-way analysis of variance, with the Tukey-Kramer multiple comparison test as the post hoc test.

maintained in 7 of these 8 genes analyzed in human synovium–derived MSCs before and after 3 weeks of chondrogenic pellet culture (Figures 3 and 4).

Interestingly, however, there was 1 exception to our overall findings. The 225-bp region of the *SDF1* promoter that lay ~1 kb upstream of the transcription start site was hypermethylated in human synovium–

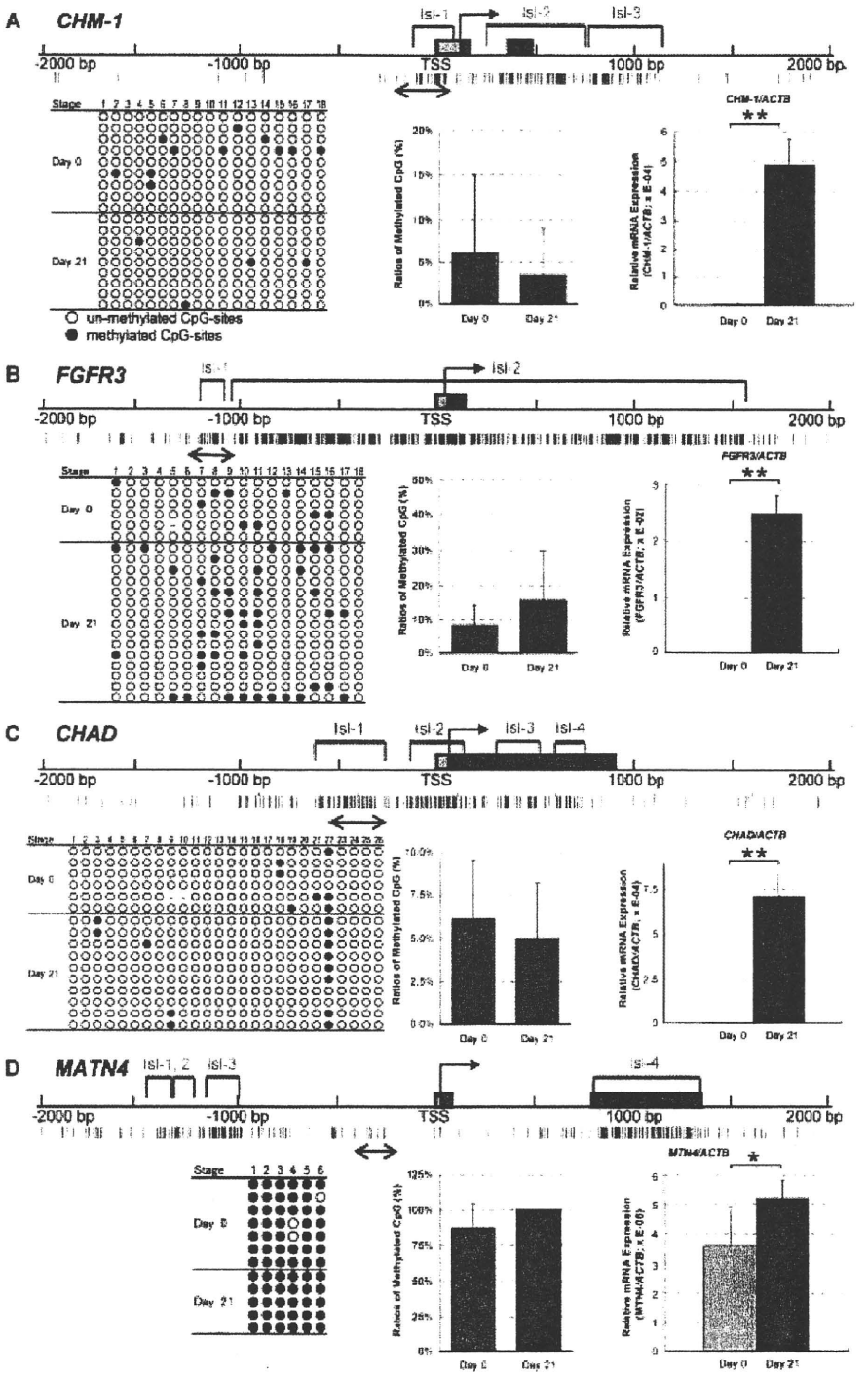

Figure 3. Analysis of CpG islands in genes that were up-regulated in chondrogenic pellet cultures. Structural features and methylation status of the transcription start site (TSS)–flanking regions (4 kb) of the selected up-regulated genes *CHM1* (**A**), *FGFR3* (**B**), *CHAD* (**C**), and *MATN4* (**D**) are shown. Structures are diagrammed as described in Figure 1. Tables show the results of bisulfite sequencing analyses of multiple bacterial colonies (– = methylation status not determined). Bar graphs show the ratio of methylated cytosine in CpG within the regions analyzed, as well as the relative mRNA expression compared with β-actin, as determined by real-time reverse transcription–polymerase chain reaction analysis. Values are the mean and SD of multiple bacterial clones. * = $P < 0.05$; ** = $P < 0.01$, by Student's *t*-test.

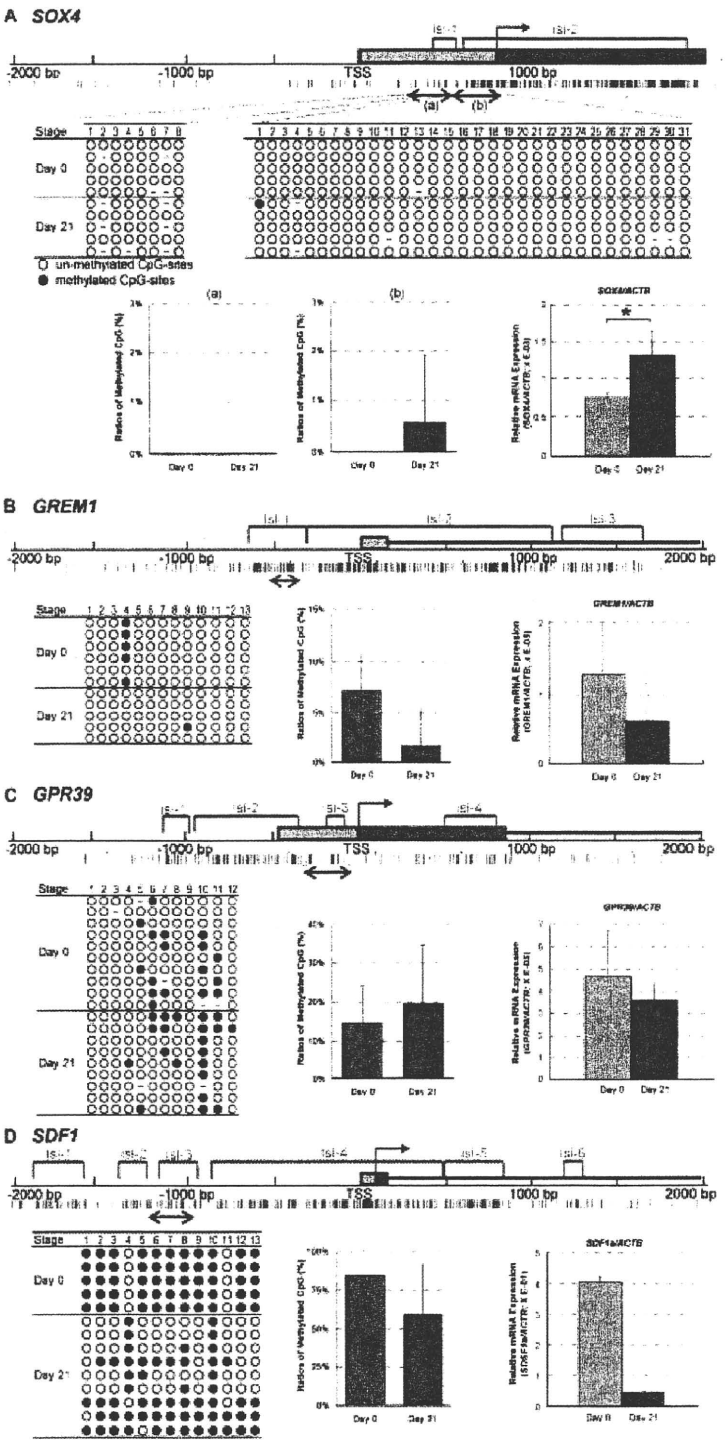

Figure 4. Analysis of CpG islands in genes that were down-regulated in chondrogenic pellet cultures. Structural features and methylation status of the transcription start site (TSS)–flanking regions (4 kb) of the selected down-regulated genes *SOX4* (**A**), *GREM1* (**B**), *GPR39* (**C**), and *SDF1* (**D**) are shown. Structures are diagrammed as described in Figure 1. Tables show the results of bisulfite sequencing analyses of multiple bacterial colonies (– = methylation status not determined). Bar graphs show the ratio of methylated cytosine in CpG within the regions analyzed, as well as the relative mRNA expression compared with β-actin, as determined by real-time reverse transcription–polymerase chain reaction analysis. Values are the mean and SD of multiple bacterial clones. * = $P < 0.05$, by Student's *t*-test.

derived MSCs, despite its relatively high CpG site density and detectable expression before the induction of chondrogenesis. The hypermethylation status (84.6%) of the *SDF1* promoter decreased after chondrogenesis (59.1%), despite silencing of its expression, as confirmed by real-time RT-PCR (Figure 4D). This observation was further supported by our bisulfite sequence analysis of the human knee articular cartilage from the patient with OA, which showed comparable levels of CpG methylation in the tangential superficial layer of the cartilage (45%), whereas in the deeper layers, much lower levels of CpG methylation were detected (13–29%) (Figure 2).

These results indicate that the methylation status of CpG-rich promoter regions is basically stable during experimental chondrogenesis and may, to a large extent, be a prerequisite for their potential for lineage commitment or differentiation. However, our results also suggest the existence of susceptible promoter regions for de novo methylation or demethylation of CpG sites during differentiation, as in the promoter region of the *SDF1* gene.

DISCUSSION

In this study, we investigated promoter DNA methylation of 10 candidate genes that encode chondrocyte phenotype–related factors with respect to epigenetic regulation during chondrogenesis of human synovium–derived MSCs. Although the hypomethylation status in 8 CpG-rich promoters was stable during the 3 weeks of chondrogenic pellet culture, we identified 1 example of a differentially methylated CpG-rich region during chondrogenesis, the promoter sequence of the *SDF1* gene.

This is the first analysis of DNA methylation status during chondrogenesis of human MSCs. Although the number of sequences examined in our study is limited in comparison to the recently reported epigenomic mapping studies (7,8), our results are consistent with the idea that high-density CpG-rich promoters are mostly hypomethylated in adult somatic cells and that the methylation status is basically stable. In fact, in those studies, only a few fractions of the CpG-rich regions were differentially methylated during different stages of stem cell differentiation (7,8). Since recent global analyses that included CpG methylation mapping studies indicated that low-density CpG site promoters tend to have more frequent differentially methylated regions as compared with CpG-rich promoters, low-density CpG regions of promoter sequences that include non-CpG islands should be examined in future studies. Nonetheless, our data support the notion that DNA methylation conditions in immature mesenchymal cells are permissive of the expression of chondrocyte phenotype–related genes in human chondrogenesis.

Embryonic regulation of CpG methylation is crucial, at least during the early stages of development. It is an essential step by which embryonic stem cells silence several key transcription factors, such as *SOX2*, octamer-binding transcription factor 3/4 (*OCT3/4*), and Nanog homeobox (*NANOG*) (29–32). Genomic imprinting is also an essential event in mammalian development, and partial disruptions of the DNA methylation machinery by genetic mutations often cause serious developmental defects (6,33–35). Cancer genomic studies have indicated the critical importance of normal methylation status in keeping cells healthy. However, in our study, the methylation status of promoter CpG islands was found to be preserved in critical genes, such as *SOX9* and *RUNX2*, during chondrogenesis. This observation may indicate a retained capability of the mesenchymal progenitor cells to change their differentiation status even after chondrogenesis, since similar observations about adipogenesis of MSCs have been reported (36–39).

Analysis of individual cellular differences in late-stage embryonic tissues might be difficult because of complex cell-type heterogeneity. Restriction landmark genomic scanning, a classic technique for global analysis of tissue-specific differentially methylated genomic regions (39,40), requires large amounts of sample DNA despite its limited sensitivity for detecting expected rare events, making microdissection of embryonic tissues neither suitable nor practical. We therefore decided to use an in vitro chondrogenesis assay of isolated MSCs. However, since MSCs do not consist of homogenous cell populations, the same situation would be true in the differentiated stage after chondrogenesis. Our use of bisulfite sequence analysis enabled the identification of individual methylated cytosines in single DNA molecules (23).

Indeed, we observed high heterogeneity of the percentage of methylation among the colonies in the promoter regions of the *FGFR3* and *SDF1* genes after 3 weeks of pellet culture (Figures 3 and 4). Interestingly, when we examined the methylation status of the same regions in freshly obtained human articular cartilage, heterogeneity seemed to be less obvious, and the percentage methylation was much higher in the *FGFR3* promoter (~50% versus 16%) and much lower in *SDF1* promoter (~25% versus 60%) (Figure 2) as compared with the results following pellet culture. This observation

may indicate that the methylation status of the in vivo specimen represents the true chondrocytic profile and that the methylation status of the in vitro sample may have been underestimated. Although there was consistency among the subcloned DNA sequences from the same experimental groups on day 0, the use of clonal populations of human MSCs may improve our results.

Our fundamental interest was to examine the epigenetic status of different types of MSCs of different tissue origins. Our finding of 1 possible example of the regulation of a target gene by CpG methylation would lead us to expect similar observations in analyses comparing various MSCs. Since MSCs have been reported to exist in various tissues, their origins might produce certain differences in the results, due to the possible inclusion of partially differentiated progenitor cells that have been committed to the cell lineage of the tissue of origin. However, future studies should also consider the possibility of heterogeneous levels of epigenetic control.

In summary, this study is the first to analyze human synovial MSCs with respect to 12 CpG-rich promoter regions of 10 chondrocyte-related candidate genes for epigenetic control during chondrogenic pellet culture. Our data on the epigenetic status of chondrocyte phenotype–related genes indicated that most of the CpG-rich promoters were hypomethylated and that this feature was mostly kept stable during MSC differentiation into chondrocytes. The observed stable epigenetic status may allow human synovial MSCs the flexibility to follow various differentiation pathways upon external stimulation, becoming, for example, osteoblasts. Since the existence of target genes for epigenetic regulation through CpG methylation has also been suggested, mechanistic studies, as well as comparisons of MSCs of different tissue origins, should be the focus of future studies.

AUTHOR CONTRIBUTIONS

Dr. Ezura had full access to all of the data in the study and takes responsibility for the integrity of the data and the accuracy of the data analysis.

Study design. Ezura, Noda.
Acquisition of data. Ezura, Sekiya, Koga, Muneta.
Analysis and interpretation of data. Ezura, Noda.
Manuscript preparation. Ezura, Sekiya, Muneta, Noda.
Statistical analysis. Ezura.

REFERENCES

1. Goldring MB, Tsuchimochi K, Ijiri K. The control of chondrogenesis. J Cell Biochem 2006;97:33–44.
2. Bernstein BE, Meissner A, Lander ES. The mammalian epigenome. Cell 2007;128:669–81.
3. Bird A. DNA methylation patterns and epigenetic memory. Genes Dev 2002;16:6–21.
4. Reik W. Stability and flexibility of epigenetic gene regulation in mammalian development. Nature 2007;447:425–32.
5. Shen Y, Chow J, Fan G. Abnormal CpG island methylation occurs during in vitro differentiation of human embryonic stem cells. Hum Mol Genet 2006;15:2623–35.
6. Robertson KD. DNA methylation and human disease. Nat Genet 2005;6:597–610.
7. Mohn F, Weber M, Rebhan M, Roloff TC, Richter J, Stadler MB, et al. Lineage-specific polycomb targets and de novo DNA methylation define restriction and potential of neuronal progenitors. Mol Cell 2008;30:755–66.
8. Meissner A, Mikkelsen TS, Hongcang G, Wernig M, Jacob H, Sivachenko A, et al. Genome-scale DNA methylation maps of pluripotent and differentiated cells. Nature 2008;755:766–70.
9. Takizawa T, Nakashima K, Namihara M, Ochiai W, Uemura A, Yanagisawa M, et al. DNA methylation is a critical cell-intrinsic determinant of astrocyte differentiation in the fetal brain. Dev Cell 2001;1:749–58.
10. Ivascu C, Wasserkort R, Lesche R, Dong J, Stein H, Thiel A, et al. DNA methylation profiling of transcription factor genes in normal lymphocyte development and lymphomas. Int J Biochem Cell Biol 2007;39:1523–38.
11. Bai S, Ghoshal K, Jacob ST. Identification of T-cadherin as a novel target of DNA methyltransferase 3B and its role in the suppression of nerve growth factor-mediated neurite outgrowth in PC12 cells. J Biol Chem 2006;281:13604–11.
12. Zuscik MJ, Baden JF, Wu Q, Sheu TJ, Schwarz EM, Drissi H, et al. 5-Azacytidine alters TGF-β and BMP signaling and induces maturation in articular chondrocytes. J Cell Biochem 2004;92:316–31.
13. Nilsson O, Mitchum RD Jr, Schrier L, Ferns SP, Barnes KM, Troendle JF, et al. Growth plate senescence is associated with loss of DNA methylation. J Endocrinol 2005;186:241–9.
14. Roach HI, Aigner T. DNA methylation in osteoarthritic chondrocytes: a new molecular target. Osteoarthritis Cartilage 2007;15:128–37.
15. Roach HI, Yamada N, Cheung KS, Tilley S, Clarke NM, Oreffo RO, et al. Association between the abnormal expression of matrix-degrading enzymes by human osteoarthritic chondrocytes and demethylation of specific CpG sites in the promoter regions. Arthritis Rheum 2005;52:3110–24.
16. Karasawa K, Kimata K, Ito K, Kato Y, Suzuki S. Morphological and biochemical differentiation of limb bud cells cultured in chemically defined medium. Dev Biol 1979;70:287–305.
17. Omi M, Sato-Maeda M, Ide H. Role of chondrogenic tissue in programmed cell death and BMP expression in chick limb buds. Int J Dev Biol 2000;44:381–8.
18. Ahrens PB, Solursh M, Reiters R. Stage-related capacity for limb chondrogenesis in cell culture. Dev Biol 1977;60:69–82.
19. Denker A, Nicoll SB, Tuan RS. Formation of cartilage-like spheroids by micromass cultures of murine C3H10T1/2 cells upon treatment with transforming growth factor-β1. Differentiation 1995;59:25–34.
20. Pittenger MF, Mackay AM, Beck SC, Jaiswal RK, Douglas R, Mosca JD, et al. Multilineage potential of adult human mesenchymal stem cells. Science 1999;284:143–7.
21. Johnstone B, Hering TM, Caplan AI, Goldberg VM, Yoo JU. In vitro chondrogenesis of bone marrow-derived mesenchymal progenitor cells. Exp Cell Res 1998;238:265–72.
22. Sakaguchi Y, Sekiya I, Yagishita K, Muneta T. Comparison of human stem cells derived from various mesenchymal tissues: superiority of synovium as a cell source. Arthritis Rheum 2005;52:2521–9.
23. Warnecke PM, Stirzaker C, Song J, Grunau C, Melki JR, Clark SJ.

Identification and resolution of artifacts in bisulfite sequencing. Methods 2002;27:101–7.
24. Shirasawa S, Sekiya I, Sakaguchi Y, Yagishita K, Ichinose S, Muneta T. In vitro chondrogenesis of human synovium-derived mesenchymal stem cells: optimal condition and comparison with bone marrow-derived cells. J Cell Biochem 2006;97:84–97.
25. Sekiya I, Vuoristo JT, Larson BL, Prockop DJ. In vitro cartilage formation by human adult stem cells from bone marrow stroma defines the sequence of cellular and molecular events during chondrogenesis. Proc Natl Acad Sci U S A 2002;99:4397–402.
26. Li LC, Dahiya R. MethPrimer: designing primers for methylation PCRs. Bioinformatics 2002;18:1427–31.
27. Pombo-Suarez M, Calaza M, Gomez-Reino JJ, Gonzalez A. Reference genes for normalization of gene expression studies in human osteoarthritic articular cartilage. BMC Mol Biol 2008;9:17.
28. Rozen S, Skaletsky HJ. Primer3 on the WWW for general users and for biologist programmers. Methods Mol Biol 2000;132:365–86.
29. Takahashi K, Yamanaka S. Induction of pluripotent stem cells from mouse embryonic and adult fibroblast cultures by defined factors. Cell 2006;126:663–76.
30. Hattori N, Nishino K, Ko YG, Hattori N, Ohgane J, Tanaka S, et al. Epigenetic control of mouse Oct-4 gene expression in embryonic stem cells and trophoblast stem cells. J Biol Chem 2004;279:17063–9.
31. Hattori N, Imao Y, Nishino K, Hattori N, Ohgane J, Yagi S, et al. Epigenetic regulation of Nanog gene in embryonic stem and trophoblast stem cells. Genes Cell 2007;12:387–96.
32. Yeo S, Jeong S, Kim J, Han JS, Han YM, Kang YK. Characterization of DNA methylation change in stem cell marker genes during differentiation of human embryonic stem cells. Biochem Biophys Res Commun 2007;359:536–42.
33. Amir RE, Van den Veyver IB, Wan M, Tran CQ, Francke U, Zoghbi HY. Rett syndrome is caused by mutations in X-linked MECP2, encoding methyl-CpG-binding protein 2. Nat Genet 1999;23:185–8.
34. Ehrlich M. The ICF syndrome, a DNA methyltransferase 3B deficiency and immunodeficiency disease. Clin Immunol 2003;109:17–28.
35. Egger G, Liang G, Aparicio A, Jones PA. Epigenetics in human disease and prospects for epigenetic therapy. Nature 2004;429:457–63.
36. Boquest AC, Noer A, Sorensen AL, Vekterud K, Collas P. CpG methylation profiles of endothelial cell-specific gene promoter regions in adipose tissue stem cells suggest limited differentiation potential toward the endothelial cell lineage. Stem Cells 2007;25:852–61.
37. Noer A, Sorensen AL, Boquest AC, Collas P. Stable CpG hypomethylation of adipogenic promoters in freshly isolated, cultured, and differentiated mesenchymal stem cells from adipose tissue. Mol Biol Cell 2006;17:3543–56.
38. Kang MI, Kim HS, Jung YC, Kim YH, Hong SJ, Kim MK, et al. Transitional CpG methylation between promoters and retroelements of tissue-specific genes during human mesenchymal cell differentiation. J Cell Biochem 2007;102:224–39.
39. Kawai J, Hirose K, Fushiki S, Hirotsune S, Ozawa N, Hara A, et al. Comparison of DNA methylation patterns among mouse cell lines by restriction landmark genomic scanning. Mol Cell Biol 1994;14:7421–7.
40. Song F, Smith JF, Kimura MT, Morrow AD, Matsuyama T, Nagase H, et al. Association of tissue-specific differentially methylated regions (TDMs) with differential gene expression. Proc Natl Acad Sci U S A 2005;102:3336–41.

THE JOURNAL OF BONE & JOINT SURGERY
JBJS

Humeral Insertion of the Supraspinatus and Infraspinatus. New Anatomical Findings Regarding the Footprint of the Rotator Cuff. Surgical Technique

Tomoyuki Mochizuki, Hiroyuki Sugaya, Mari Uomizu, Kazuhiko Maeda, Keisuke Matsuki, Ichiro Sekiya, Takeshi Muneta and Keiichi Akita

J Bone Joint Surg Am. 2009;91:1-7. doi:10.2106/JBJS.H.01426

Humeral Insertion of the Supraspinatus and Infraspinatus. New Anatomical Findings Regarding the Footprint of the Rotator Cuff

Surgical Technique

By Tomoyuki Mochizuki, MD, Hiroyuki Sugaya, MD, Mari Uomizu, MD, Kazuhiko Maeda, MD, Keisuke Matsuki, MD, Ichiro Sekiya, MD, Takeshi Muneta, MD, and Keiichi Akita, MD

Investigation performed at the Unit of Clinical Anatomy, Graduate School, Tokyo Medical and Dental University, Tokyo, Japan

The original scientific article in which the surgical technique was presented was published in JBJS Vol. 90-A, pp. 962-9, May 2008

ABSTRACT FROM THE ORIGINAL ARTICLE

BACKGROUND: It is generally believed that the supraspinatus is the most commonly involved tendon in rotator cuff tears. Clinically, however, atrophy of the infraspinatus muscle is frequently observed in patients with even small to medium-size rotator cuff tears. This fact cannot be fully explained by our current understanding of the anatomical insertions of the supraspinatus and infraspinatus. The purpose of this study was to reinvestigate the humeral insertions of these tendons.

METHODS: The study included 113 shoulders from sixty-four cadavers. The humeral insertion areas of the supraspinatus and infraspinatus were investigated in ninety-seven specimens. In sixteen specimens, all muscular portions of the supraspinatus and infraspinatus were removed, leaving the tendinous portions intact, in order to define the specific characteristics of the tendinous portion of the muscles. Another twenty-six shoulders were used to obtain precise measurements of the footprints of the supraspinatus and infraspinatus.

RESULTS: The supraspinatus had a long tendinous portion in the anterior half of the muscle, which always inserted into the anteriormost area of the highest impression on the greater tuberosity and which inserted into the superiormost area of the lesser tuberosity in 21% of the specimens. The footprint of the supraspinatus was triangular in shape, with an average maximum medial-to-lateral length of 6.9 mm and an average maximum anteroposterior width of 12.6 mm. The infraspinatus had a long tendinous portion in the superior half of the muscle, which curved anteriorly and extended to the anterolateral area of the highest impression of the greater tuberosity. The footprint of the infraspinatus was trapezoidal in shape, with an average maximum medial-to-lateral length of 10.2 mm and an average maximum anteroposterior width of 32.7 mm.

CONCLUSIONS: The footprint of the supraspinatus on the greater tuberosity is much smaller than previously believed, and this area of the greater tuberosity is actually occupied by a substantial amount of the infraspinatus.

LEVEL OF EVIDENCE: The present study suggests that rotator cuff tears that were previously thought to involve only the supraspinatus tendon may in fact have had a substantial infraspinatus component as well.

ORIGINAL ABSTRACT CITATION: "Humeral Insertion of the Supraspinatus and Infraspinatus. New Anatomical Findings Regarding the Footprint of the Rotator Cuff" (2008;90:962-9).

DISCLOSURE: In support of their research for or preparation of this work, one or more of the authors received, in any one year, outside funding or grants in excess of $10,000 from KAKENHI (19890069) Grant-in-Aid for Young Scientists (Start-up). Neither they nor a member of their immediate families received payments or other benefits or a commitment or agreement to provide such benefits from a commercial entity. No commercial entity paid or directed, or agreed to pay or direct, any benefits to any research fund, foundation, division, center, clinical practice, or other charitable or nonprofit organization with which the authors, or a member of their immediate families, are affiliated or associated.

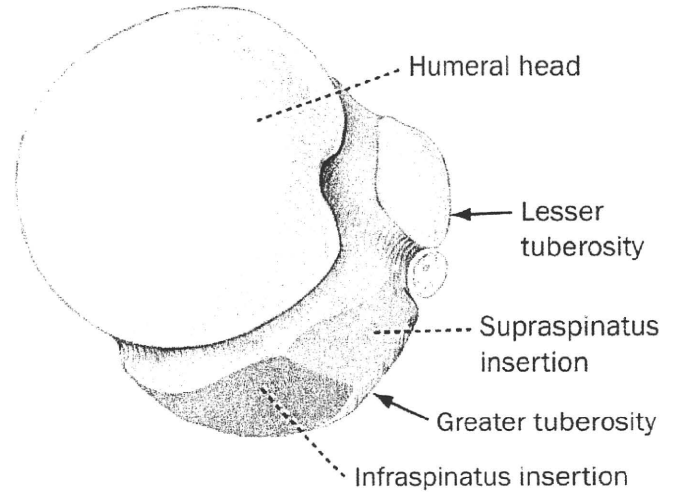

FIG. 1-A

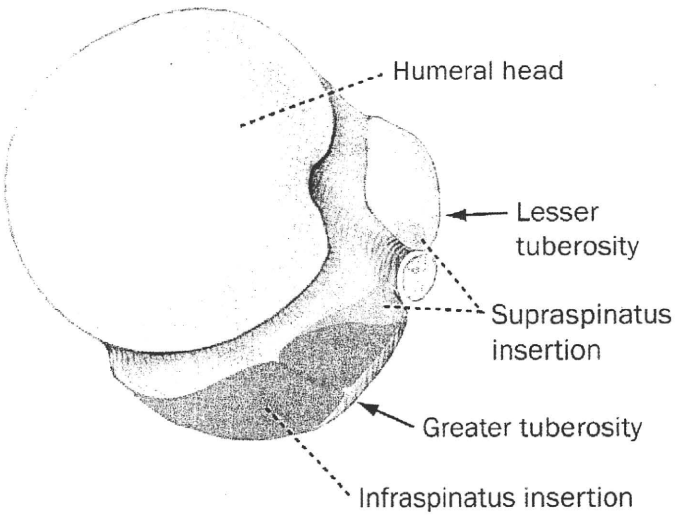

FIG. 1-B

Illustrations of the superior aspect of the right humerus, showing the humeral insertions of the supraspinatus and infraspinatus. *A:* An illustration based on the generally accepted concept of the anatomy of the humeral insertions. The supraspinatus is shown to insert into the superior facet and the infraspinatus, into the middle facet (middle impression) of the greater tuberosity. *B:* An illustration based on the findings of the present study. The insertion area of the infraspinatus occupies approximately half of the superior facet and the entire middle facet of the greater tuberosity. The insertion area of the supraspinatus is located at the anteromedial region of the superior facet and is sometimes located at the superiormost area on the lesser tuberosity.

INTRODUCTION

Previous reports regarding rotator cuff tears have stated that most tears primarily involve the supraspinatus and not the infraspinatus[1-3]. In the present study, however, the footprint of the supraspinatus was found to be limited to the anteromedial aspect of the superior facet (the highest impression) of the greater tuberosity, while that of the infraspinatus occupied the majority of the greater tuberosity including the anterolateral aspect of the superior facet (Fig. 1). These results imply that the infraspinatus tendon may be involved in small to medium-size rotator cuff tears in a much higher proportion than previously appreciated.

On the basis of these findings, when we repair full-thickness rotator cuff tears, we believe that it is very important to bring the posteromedial leaf anterolaterally and reattach it to the anterior portion of the greater tuberosity in order to

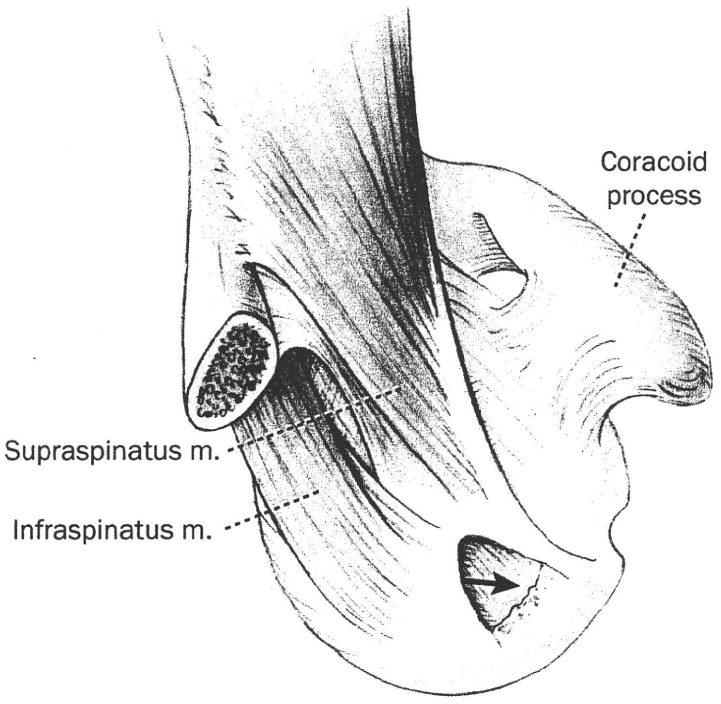

FIG. 2-A

A: A typical full-thickness rotator cuff tear that involves the supraspinatus and infraspinatus. *B:* The posterior leaf is easily mobilized anterolaterally (arrow). In this situation, margin convergence repair is not recommended. *C:* The posterior leaf is reattached to the anterolateral portion of the superior facet of the greater tuberosity. The repair is augmented by applying side-to-side stitches to the anterior leaf.

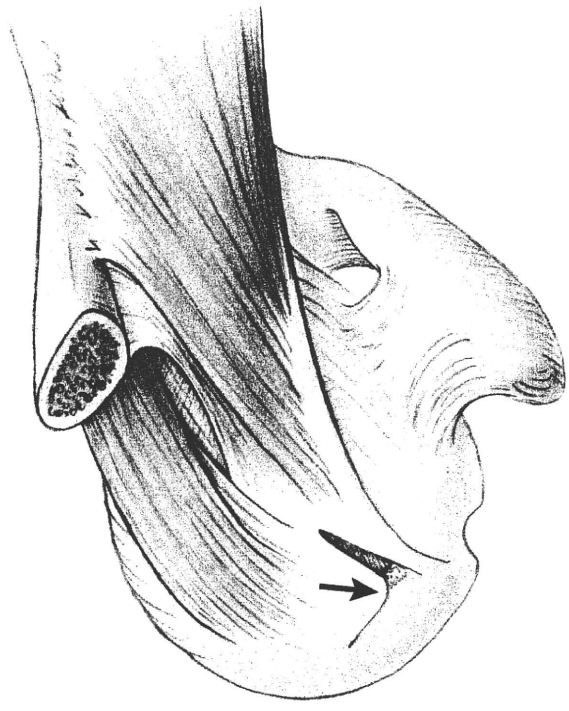

FIG. 2-B

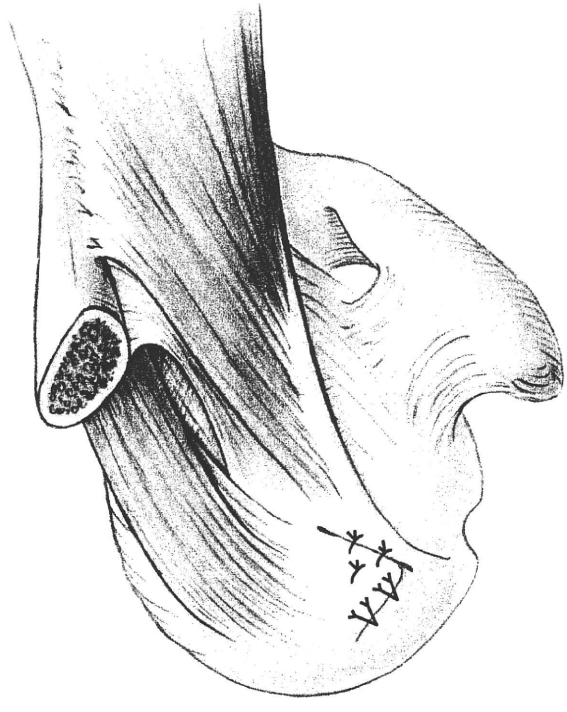

FIG. 2-C

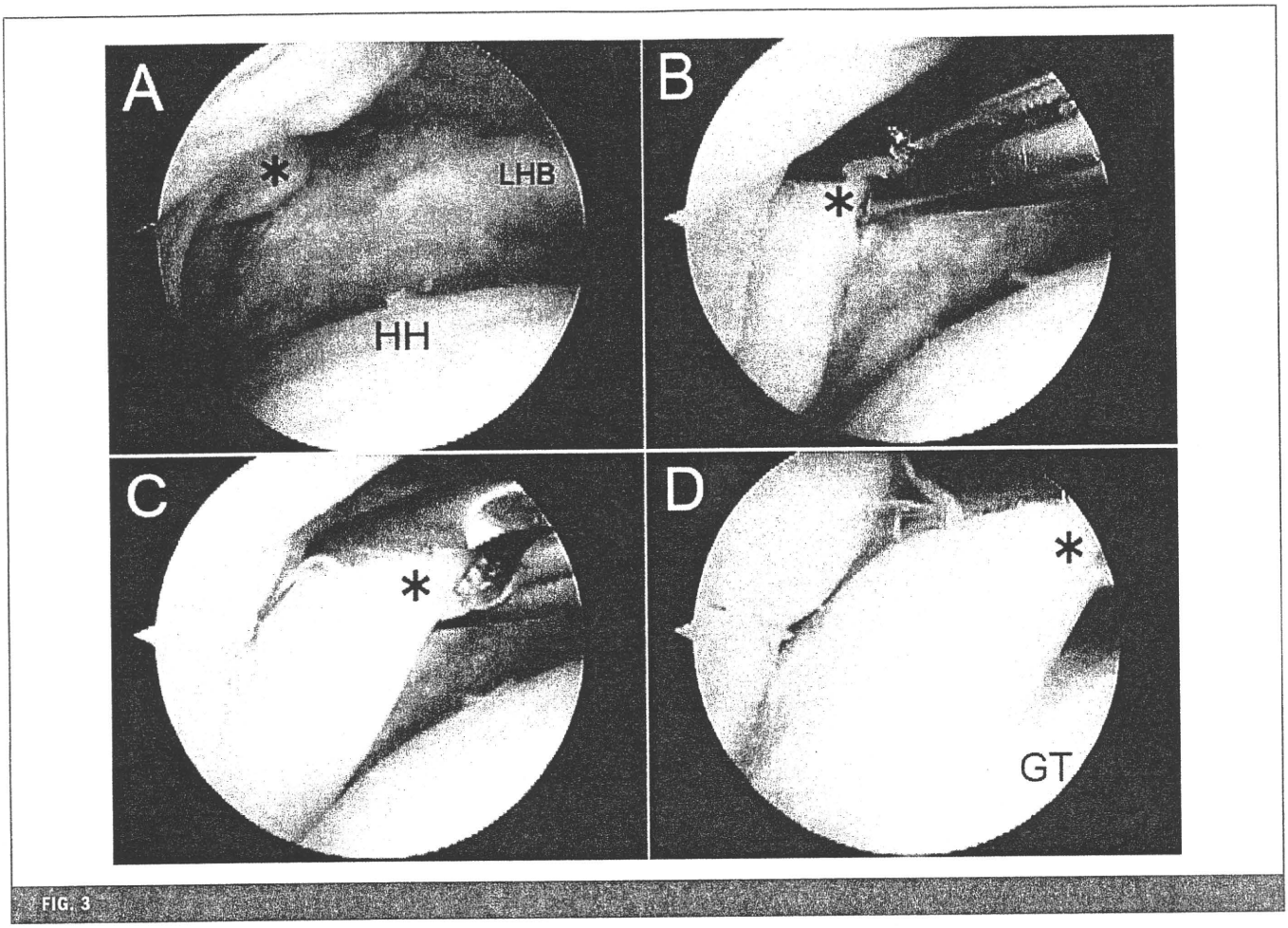

FIG. 3

A: A large delaminated rotator cuff tear viewed from the posterolateral portal (right shoulder). *B:* A grasper holds the deep layer (asterisk) of the posterior leaf. *C:* The posterior leaf is easily mobilized anterolaterally. *D:* The posterior leaf is reattached to the anterior portion of the greater tuberosity. GT = greater tuberosity, HH = humeral head, and LHB = long head of biceps tendon.

achieve a balanced anatomical repair.

In the present report, we describe the pearls and pitfalls for the balanced anatomical repair of full-thickness rotator cuff tears on the basis of the results of our anatomical study.

SURGICAL TECHNIQUE

Arthroscopic Evaluation

The patient is seated in the beach-chair position while under general anesthesia. A posterior portal is established for the initial assessment of the glenohumeral joint. An anterior portal through the rotator interval is established as the working portal for the treatment of intra-articular lesions. The tear size and the presence of delamination are carefully determined. The arthroscope is then removed from the glenohumeral joint and is redirected into the subacromial space. A lateral portal and a posterolateral portal are also established. Any pathological bursal tissue that impedes clearance of the space is removed, and an arthroscopic subacromial decompression is performed to create a flat acromial undersurface. Osteophytes extending from the inferior part of the acromioclavicular joint and the distal end of the clavicle are also removed as necessary. The posterolateral portal is used mainly as a viewing portal in these procedures.

Repair of a Full-Thickness Tear

The tear size and pattern are again evaluated, and the mobility and repairability of the torn rotator cuff are then estimated.

When a full-thickness tear is repaired, the mobility of the posterior leaf is typically better than that of the central or anterior leaf. If the tear is a full-thickness u-shaped tear (Fig. 2, *A*), it is easily reduced by pulling the posterior leaf anterolaterally toward the anterior edge of the greater tuberosity (Figs. 2, *B* and 3). If the mobility of the tendon is insufficient in a larger tear, a tendon mobilization procedure is performed. This includes a capsulotomy at the undersurface of the supraspinatus and infraspinatus and release of the coracohumeral ligament at the origin of the posterior aspect of the coracoid process. However, we do not perform the so-called rotator interval slide. The footprint of the greater tuberosity is débrided in order to expose cortical bone, but excessive removal of bone is avoided. A double row repair of the posterior leaf as well as a side-to-side repair are then performed (Fig. 2, *C*), instead of performing a so-called margin convergence repair.

Advance the Posterior Leaf Anterolaterally

In our anatomical study, the supraspinatus inserted into the most anterior aspect of the greater tuberosity in normal specimens without a rotator cuff tear (Fig. 1). In addition, in most cadaver specimens with a rotator cuff tear, the infraspinatus was torn and retracted posteromedially (Fig. 4). Therefore, the most critical concept in our procedure is to bring the torn edge of the infraspinatus anterolaterally and reattach it to the anterior area of the greater tuberosity (Figs. 2 and 3).

Margin Convergence Repair May Not Be the Preferred Procedure

In the repair of the so-called u-shaped tear and some of the crescent-type tears (Fig. 2), the margin convergence procedure, which is a direct side-to-side suture of both the anterior and posterior leafs, is commonly preferred by many surgeons[4]. It is true that the margin conver-

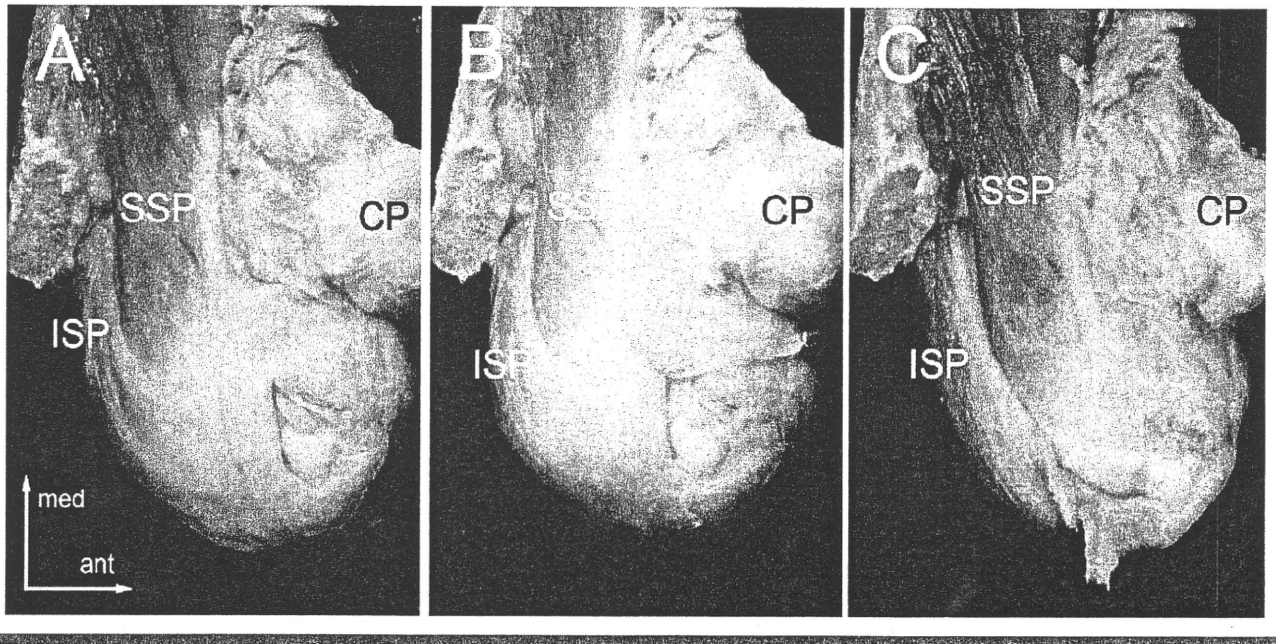

FIG. 4

A: A typical full-thickness rotator cuff tear localized to the anteromedial portion seen in a cadaver shoulder. This is generally thought to be an isolated supraspinatus tear. *B:* When the overlapping coracohumeral ligament is removed, the tear also appears to involve the anterior half of the infraspinatus tendon. *C:* After the anterior half of the infraspinatus tendon is removed, only a minor tear of the posterior portion of the supraspinatus tendon is observed. However, the anterior portion of the supraspinatus tendon appears to be intact. CP = coracoid process, ISP = infraspinatus, SSP = supraspinatus, ant = anterior, and med = medial.

gence procedure is sometimes very effective in reducing the size of the u-shaped tear. However, on the basis of our anatomical study, it is evident that the posterior leaf of a so-called L-shaped tear has retracted posteromedially to alter the final configuration of the tear to a u-shaped lesion in the chronic stage. Therefore, we think that surgeons should be more careful in choosing to apply the margin convergence technique in u-shaped tears[5]. We strongly recommend that the mobility of the torn rotator cuff be evaluated to determine the repair design because the posterior leaf is normally very mobile compared with the anterior or the central leaf; this would allow conversion of many u-shaped lesions to L-shaped tears that are amenable to successful anatomical repair by mobilization of the posterior infraspinatus and supraspinatus flap.

Preserve the "Comma" During a Repair Involving the Subscapularis

Lo and Burkhart reported on the utility of the comma sign, which is a comma-shaped arc of tissue located at the superolateral border of the subscapularis, delineating the retracted edge of the subscapularis[6] (Fig. 5, *A*). They also suggested that the comma is actually the remnant of the medial sling of the biceps, which is composed of fibers of the medial head of the coracohumeral ligament as well as a portion of the superior glenohumeral ligament. We reported that the supraspinatus has a long intramuscular tendinous portion located in the anterior half of the muscle, which was found to insert into the most superior area of the lesser tuberosity in 21% of our specimens (Fig. 5, *B*). We believe that the comma represents this tendinous portion of the supraspinatus, which connects the supraspinatus and the subscapularis. Therefore, when we repair the subscapularis, it is very important to preserve this connecting tissue to avoid postoperative structural failure as well as to restore the function of the supraspinatus.

Rotator Interval Slide May Not Be a Preferable Procedure

The interval slide, either anteriorly or posteriorly, has been reported to be a very effective procedure for mobilization of retracted massive rotator cuff tears[7,8]. However, as we demonstrated in our anatomical study, the distal end of the infraspinatus tendon courses anterolaterally and inserts into the anterolateral portion of the superior facet. Further, some of the tendinous fibers of the supraspinatus run across the bicipital groove and insert into the lesser tuberosity. We believe that these structures work as a horizontal link of each rotator cuff tendon, especially in large retracted tears. Therefore, it is very important to preserve these structural interconnections in order to avoid failures after repair.

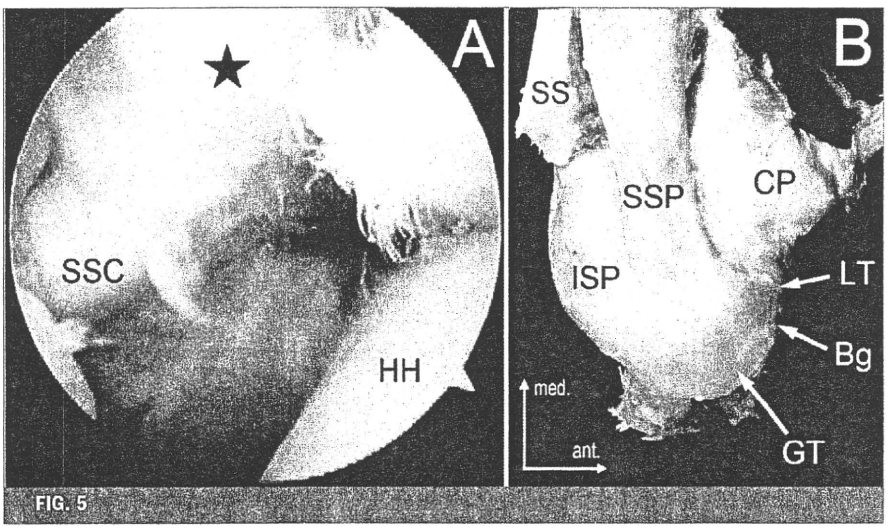

FIG. 5

A: The comma (black star) viewed from the posterior portal (right shoulder). The comma-shaped arc of tissue leads to the superolateral edge of the subscapularis tendon. *B:* The fibers from the supraspinatus tendon insert on the lesser tuberosity (superior aspect of the right shoulder). SSC = subscapularis, HH = humeral head, Bg = bicipital groove, CP = coracoid process, GT = greater tuberosity, ISP = infraspinatus, LT = lesser tuberosity, SS = scapular spine, SSP = supraspinatus, med = medial, and ant = anterior.

CRITICAL CONCEPTS

INDICATIONS:

This procedure is applicable for every reparable rotator cuff tear.

CONTRAINDICATIONS:

There is no specific contraindication to this procedure if the tear is reparable.

PITFALLS:

Margin convergence repair is not the preferred method for repairing u-shaped rotator cuff tears because most u-shaped types of tears are chronic and represent an advanced stage of the L-shaped tear. Surgeons should evaluate the mobility of the posterior leaf of the tear before applying the margin convergence technique.

The rotator interval slide as a method to increase mobility in large retracted tears is not preferred because the tendinous fibers intermingle with each other and work as a horizontal link at the distal end of the rotator cuff tear. If surgeons violate this structure, the risk of postoperative failure may be increased.

AUTHOR UPDATE:

Through our clinical experience, we believe that, normally, the posterior leaf of the torn rotator cuff is more mobile compared with the anterior or central leaf. Furthermore, we have wondered why the integrity of the repair is relatively poor after the use of the margin convergence suture technique and the rotator interval slide in larger tears. Therefore, we are very reluctant to use the margin convergence technique for large u-shaped tears or to use the rotator interval slide as a mobilization procedure for large retracted tears.

Tomoyuki Mochizuki, MD
Mari Uomizu, MD
Ichiro Sekiya, MD
Takeshi Muneta, MD
Keiichi Akita, MD
Unit of Clinical Anatomy (M.U. and K.A.) and Section of Orthopaedic Surgery (T. Mochizuki, I.S., and T. Muneta), Graduate School, Tokyo Medical and Dental University, 1-5-45 Yushima, Bunkyo-ku, Tokyo 113-8519, Japan. E-mail address for T. Mochizuki: mochizuki.orj@tmd.ac.jp. E-mail address for K. Akita: akita.fana@tmd.ac.jp

Hiroyuki Sugaya, MD
Kazuhiko Maeda, MD
Funabashi Orthopaedic Sports Medicine Center, 1-833 Hazama, Funabashi, Chiba 274-0822, Japan

Keisuke Matsuki, MD
Department of Orthopedic Surgery, Teikyo University Chiba Medical Center, 3426-3 Anegasaki Ichihara, Chiba 299-0111, Japan

The line drawings in this article are the work of Joanne Haderer Müller of Haderer & Müller (biomedart@haderermuller.com).

REFERENCES

1. Jerosch J, Müller T, Castro WH. The incidence of rotator cuff rupture. An anatomic study. Acta Orthop Belg. 1991;57:124-9.

2. Lehman C, Cuomo F, Kummer FJ, Zuckerman JD. The incidence of full thickness rotator cuff tears in a large cadaveric population. Bull Hosp Jt Dis. 1995;54:30-1.

3. Harryman DT 2nd, Mack LA, Wang KY, Jackins SE, Richardson ML, Matsen FA 3rd. Repairs of the rotator cuff. Correlation of functional results with integrity of the cuff. J Bone Joint Surg Am. 1991;73:982-9.

4. Burkhart SS, Athanasiou KA, Wirth MA. Margin convergence: a method of reducing strain in massive rotator cuff tears. Arthroscopy. 1996;12:335-8.

5. Sugaya H, Maeda K, Matsuki K, Moriishi J. Repair integrity and functional outcome after arthroscopic double-row rotator cuff repair. A prospective outcome study. J Bone Joint Surg Am. 2007;89:953-60.

6. Lo IK, Burkhart SS. The comma sign: an arthroscopic guide to the torn subscapularis tendon. Arthroscopy. 2003;19:334-7.

7. Lo IK, Burkhart SS. The interval slide in continuity: a method of mobilizing the anterosuperior rotator cuff without disrupting the tear margins. Arthroscopy. 2004;20:435-41.

8. Tauro JC. Arthroscopic repair of large rotator cuff tears using the interval slide technique. Arthroscopy. 2004;20:13-21.

STEM CELLS®
TISSUE-SPECIFIC STEM CELLS

Intra-articular Injected Synovial Stem Cells Differentiate into Meniscal Cells Directly and Promote Meniscal Regeneration Without Mobilization to Distant Organs in Rat Massive Meniscal Defect

MASAFUMI HORIE,[a] ICHIRO SEKIYA,[b] TAKESHI MUNETA,[a,c] SHIZUKO ICHINOSE,[d] KENJI MATSUMOTO,[e] HIROHISA SAITO,[e] TAKASHI MURAKAMI,[f] EIJI KOBAYASHI[f]

[a]Section of Orthopedic Surgery, [b]Section of Cartilage Regeneration, Graduate School, [c]Global Center of Excellence Program and International Research Center for Molecular Science in Tooth and Bone Diseases, and [d]Instrumental Analysis Research Center, Tokyo Medical and Dental University, Tokyo, Japan; [e]Department of Allergy and Immunology, National Research Institute for Child Health and Development, Tokyo, Japan; [f]Division of Organ Replacement Research, Center for Molecular Medicine, Jichi Medical University, Tochigi, Japan

Key Words. Mesenchymal stem cells • Synovium • Meniscus • Luciferase • LacZ • Cell transplantation

ABSTRACT

Osteoarthritis in the knees, which can be caused by meniscal defect, constitutes an increasingly common medical problem. Repair for massive meniscal defect remains a challenge owing to a lack of cell kinetics for the menisci precursors in knee joint. The synovium plays pivotal roles during the natural course of meniscal healing and contains mesenchymal stem cells (MSCs) with high chondrogenic potential. Here, we investigated whether intra-articular injected synovium-MSCs enhanced meniscal regeneration in rat massive meniscal defect. To track the injected cells, we developed transgenic rats expressing dual luciferase (Luc) and LacZ. The cells derived from synovium of the rats demonstrated colony-forming ability and multipotentiality, both characteristics of MSCs. Hierarchical clustering analysis revealed that gene expression of meniscal cells was closer to that of synovium-MSCs than to that of bone marrow-MSCs. Two to 8 weeks after five million Luc/LacZ+ synovium-MSCs were injected into massive meniscectomized knee of wild-type rat, macroscopically, the menisci regenerated much better than it did in the control group. After 12 weeks, the regenerated menisci were LacZ positive, produced type 2 collagen, and showed meniscal features by transmission electron microscopy. In in-vivo luminescence analysis, photons increased in the meniscus-resected knee over a 3-day period, then decreased without detection in all other organs. LacZ gene derived from MSCs could not be detected in other organs except in synovium by real-time PCR. Synovium-MSCs injected into the massive meniscectomized knee adhered to the lesion, differentiated into meniscal cells directly, and promoted meniscal regeneration without mobilization to distant organs. STEM CELLS *2009;27:878–887*

Disclosure of potential conflicts of interest is found at the end of this article.

INTRODUCTION

The meniscus is a wedge-shaped semilunar fibrocartilage that lies between the weight bearing joint surfaces of the femur and the tibia. For symptomatic meniscus injury, a meniscectomy is often performed. This, however, often leads to osteoarthritis [1]. Meniscal suture to preserve its function is limited for its indication, and the result is not always satisfactory due to poor healing of the meniscus. Despite other therapeutic attempts [2], problems related to its effectiveness and invasion persist. A novel strategy for meniscus injury remains necessary.

Mesenchymal stem cells (MSCs) are postulated to participate in tissue homoeostasis, remodeling, and repair by ensuring the replacement of mature cells lost to physiological turnover, senescence, injury, or disease. Stem cell populations are found in most adult tissues, and in general, their differentiation potential may reflect the local cell population. Developmentally, intra-articular tissues are differentiated from common progenitors, referred to as common interzone cells [3]. Synovium-MSCs have high

Author contributions: M.H.: conception and design, data analysis, collection of data, and manuscript writing; I.S.: conception and design, financial support, manuscript writing, final approval of manuscript; T. Muneta: conception and design, financial support, and administrative support; S.I.: electron microscopy; K.M.: microarray and real-time PCR; H.S.: microarray and real-time PCR; T. Murakami: provision of study material and manuscript writing; E.K.: conception and design, financial support, administrative support, provision of study material, manuscript writing.

Correspondence: Ichiro Sekiya, M.D., Ph.D., Section of Cartilage Regeneration, Graduate School, Tokyo Medical and Dental University, 1-5-45 Yushima, Bunkyo-Ku, Tokyo 113-8519, Japan. Telephone: +81-3-5803-4675; Fax: +81-3-5803-0266; e-mail: sekiya.orj@tmd.ac.jp; or Eiji Kobayashi, M.D., Ph.D., Division of Organ Replacement Research, Center for Molecular Medicine, Jichi Medical University, 3311-1 Yakushiji, Shimotsuke, Tochigi 329-0498, Japan. Telephone: +81-285-58-7446; Fax: +81-285-44-5365; e-mail: eijikoba@jichi.ac.jp Received July 16, 2008; accepted for publication December 9, 2008; first published online in STEM CELLS *EXPRESS* January 8, 2009. 1066-5099/2009/$30.00/0 doi: 10.1634/stemcells.2008-0616

chondrogenic potential [4, 5], clinically increase in number in synovial fluid after intra-articular tissue injury to contribute to its repair in part [6] and expand in the presence of pure synovial fluid in tissue cultures of the synovium [7]. Synovial tissue may serve as a reservoir of stem cells that mobilize following injury and migrate to the wound site where, in cooperation with local cells, they participate in the repair response.

Thus, during the natural course of meniscal repair, synovium-MSCs are a potential cell source. Here, we investigated whether intra-articular injected synovium-MSCs enhanced meniscal regeneration in rat massive meniscal defect. Dual colored transgenic (Tg) rats expressing luciferase and LacZ (Luc/LacZ) were created for this study so that the fate of transplanted cells could be traced dynamically and precisely.

Materials and Methods

Establishment of Dual Colored Transgenic Rat

Dual colored Tg rats expressing luciferase and Lac-Z were created by cross-breeding ROSA/luciferase Tg Lewis rats [8] with ROSA/LacZ Lewis rats [9]. The expression of luciferase was detected by an in vivo bioimaging system, and the expression of LacZ was detected by X-gal staining (detailed later). The F1 hybrids between ROSA/luciferase Tg and ROSA/LacZ Lewis rat neonate were imaged after *intraperitoneal injection of* D-luciferin (30 mg/kg per body weight) (potassium salt; Biosynth, Postfach, Switzerland, http://www.biosynth.com), and then they were stained with X-gal. In the same manner, luciferase and LacZ expressions were examined in various tissues of these rats. Approximately one-fourth of these F1 hybrids expressed luciferase and LacZ in the whole body. We used these "dual colored" F1 hybrids expressing both luciferase and LacZ (Luc/LacZ) for the donor of MSCs.

MSCs Preparation

All experiments were conducted in accordance with the institutional guidelines for the care and use of experimental animals of Tokyo Medical and Dental University and Jichi Medical University. The synovial membranes of bilateral knee joints were excised, minced, and digested for 3 hours at 37°C with type V collagenase (0.2%; Sigma-Aldrich, St. Louis, MO, http://www.sigmaaldrich.com), and passed through a 40-μm filter (Becton Dickinson, Franklin Lakes, NJ, http://www.bd.com). Bone marrow was extruded by inserting a 22-gauge needle into the shaft of the femur and tibia bone and flushed out. Synovium and bone marrow cells were cultured in a complete medium (αMEM; Invitrogen, Carlsbad, CA, http://www.invitrogen.com; 20% FBS; Invitrogen; 100 units per milliliter penicillin, 100 μg/ml streptomycin, and 2 mM L-glutamine; Invitrogen) for 14 days. Then the cells were replated at 100 cells/cm^2, cultured for 14 days, and frozen at −80°C as passage 1. The stocked cells were rapidly thawed in a water bath at 37°C, plated in a 150 cm^2 dish, and harvested after 5 days. Then the cells were replated at 100 cells/cm^2, cultured for 14 days, and collected for further analyses [5]. For colony-forming assay, 100 cells were plated in 60 cm^2 dishes and cultured for 14 days. The dishes were stained with X-gal, and the same dishes were then stained with 0.5% Crystal Violet.

In Vitro Differentiation Assay

For adipogenesis, the cells were cultured in the adipogenic medium that consisted of a complete medium supplemented with 0.5 μM dexamethasone, 0.5 mM isobutylmethylxanthine, and 50 μM indomethacin. After 4 days, the adipogenic cultures were stained with 0.3% Oil Red-O solution or X-gal solution [10].

For osteogenesis, the cells were cultured in the calcification medium in the presence of 100 nM dexamethasone, 10 mM β-glycerophosphate, and 50 μM ascorbic acid. After an additional 6 weeks, the dishes were stained with 0.5% Alizarin Red solution or X-gal solution.

For in vitro chondrogenesis, 8×10^5 cells were placed in a 15 ml polypropylene tube (BD Falcon, Bedford, MA, http://www.bdbiosciences.com) and pelleted by centrifugation at 450*g* for 10 minutes. The pellets were cultured for 21 days in chondrogenic media, which contained 500 ng/ml BMP-2 (Astellas Pharma Inc., Tokyo, Japan, http://www.astellas.com), in addition to high-glucose Dulbecco's modified Eagle's medium (Invitrogen) supplemented with 10 ng/ml transforming growth factor-β3 (TGF-β3) (R&D Systems Inc., Minneapolis, MN, http://www.rndsystems.com), 10^{-7} M dexamethasone, 50 μg/ml ascorbate-2-phosphate, 40 μg/ml proline, 100 μg/ml pyruvate, and 50 mg/ml ITS+TMPremix (Becton Dickinson). For histological analysis, the pellets were embedded in paraffin, cut into 5-μm sections, and stained with 1% Toluidine Blue [11].

Flow Cytometry

Synovium-MSCs at passage 3 were harvested 14 days after plating. One million cells were suspended in 500 μl phosphate buffered saline (PBS) containing 20 ng/ml fluorescein isothiocyanate (FITC) or phycoerythrin (PE)-coupled antibodies against CD11b, CD45, CD90 (Becton Dickinson), CD34 (Santa Cruz Biotechnology Inc., Santa Cruz, CA, http://www.scbt.com), and CD29 (BioLegend, San Diego, CA, http://www.biolegend.com) As an isotype control, FITC- or PE-coupled nonspecific mouse IgG (Becton Dickinson) was substituted for the primary antibody. After incubation for 30 minutes at 4°C, the cells were washed with PBS and resuspended in 1 ml PBS for analysis. Cell fluorescence was evaluated by flow cytometry in a FACSCalibur instrument (Becton Dickinson); data were analyzed by using CellQuest software (Becton Dickinson).

Oligonucleotide Microarray

For rat meniscal cells, menisci were minced, digested for 3 hours at 37°C with type II collagenase (0.2%; Sigma), and passed through a 40 μm filter (Becton Dickinson). Nucleated cells were plated at 100 cells/cm^2 and cultured in a complete medium. Total RNA was isolated from passage 1 colony-formed cells derived from the synovium, bone marrow [5], and meniscus with the RNeasy Total RNA Mini Kit (Qiagen, Valencia, CA, http://www1.qiagen.com).

A comprehensive microarray analysis was performed using 3 μg of total RNA from each sample and GeneChip Rat 230 2.0 probe arrays (Affymetrix, Santa Clara, CA, http://www.affymetrix.com) [12]. Data analysis was performed with GeneSpring software version 7.2 (Agilent Technologies, Palo Alto, CA, http://www.agilent.com). To normalize the variations in staining intensity among chips, the "Signal" values for all genes on a given chip were divided by the median value for the expression of all genes on the chip. To eliminate genes containing only a background signal, genes were selected only if the raw values of the "Signal" were more than 30, and expression of the gene was judged to be "Present" by the GeneChip Operating Software version 1.4 (Affymetrix). After elimination, expression data of a total of 14,882 probe sets were employed for further analysis. A hierarchical-clustering analysis was performed using a minimum distance value of 0.001, a separation ratio of 0.5, and the standard definition of the correlation distance. A dendrogram was obtained from a hierarchically clustering analysis using average linkage and distance metric equal to one minus the Pearson correlation applied to the microarray data [13].

Meniscectomy and MSCs Injection

Wild-type male Lewis rats at 12 weeks of age (Charles River, Yokohama, Japan, http://www.crj.co.jp) were used (n = 27). Under anesthesia, a straight incision was made on the anterior side of bilateral knee, the anteromedial side of the joint capsule was cut, and the anterior horn of the medial meniscus was dislocated anteriorly with a forceps. The meniscus was then cut vertically at the level of medial collateral ligament, and the anterior half of medial meniscus was excised. The dislocated meniscus was removed and the wound was closed in layers. Immediately after the skin incision was closed, a 27-gauge needle was inserted

at the center of the triangle formed by the medial side of the patellar ligament, the medial femoral condyle, and the medial tibial condyle, toward the intercondylar space of the femur. Then 5 × 10^6 Luc/LacZ$^+$ synovium-MSCs (n = 14) or bone marrow-MSCs (n = 9) in 50 μl PBS were injected into the right knee joint. For the control, the same volume of PBS was injected into the left knee. The rats were allowed to walk freely in the cage.

For control of in vivo Imaging analysis, 5 × 10^6 Luc/LacZ$^+$ synovium-MSCs were injected into the normal right knee of the wild-type Lewis rats (n = 4).

Histology and Detection of LacZ Expression

The whole medial meniscus was collected at 2, 4, 8, and 12 weeks after MSCs injection (n = 3 each time point). The samples were fixed with a fixative solution (0.2% glutaraldehyde, 2 mM $MgCl_2$, and 5 mM EGTA) in PBS for 10-30 minutes at room temperature and washed three times in a washing solution (2 mM $MgCl_2$, 0.01% sodium deoxycholate, and 0.02% Nonidet P40) in PBS. Then they were treated with an X-gal staining solution (1 mg/ml of 5-bromo-4-chloro-3-indolyl-β-D-galactopyranoside, 2 mM $MgCl_2$, and 5 mM potassium hexacyanoferrate [III], 5 mM potassium hexacyanoferrate [II] trihydrate) at 37°C for 3 hours. They were subsequently fixed again in 4% paraformaldehyde and decalcified with 0.5 M EDTA (pH 7.5) for 3 days at 4°C, followed by a gradient replacement with 20% sucrose for 24 hours at 4°C, and then evaluated by Toluidine Blue or Eosin staining of paraffin sections.

Immunostaining

Sections were pretreated with 0.4 mg/ml proteinase K (DAKO, Carpinteria, CA, http://www.dakousa.com) in Tris-HCl for 15 minutes at room temperature for optimal antigen retrieval. Residual enzymatic activity was removed by washes in PBS, and nonspecific staining was blocked with PBS containing 10% normal horse serum for 20 minutes at room temperature. A primary anti-rat monoclonal antibody against human type II collagen (1 : 200 dilution with PBS containing 1% BSA; Daiichi Fine Chemical, Toyama, Japan, http://www.daiichi-fcj.co.jp) was applied to the section which was incubated at room temperature for 1 hour and rinsed again with PBS. Immunostaining was detected by Vectastain ABC reagent (Vector Laboratories, Burlingame, CA; http://www.vectorlabs.com), followed by diaminobenzidine staining.

In Vivo Bioluminescent Imaging

A noninvasive bioimaging system IVIS (Xenogen, Alameda, CA, http://www.caliperls.com) was used for analysis using IGOR (WaveMetrics, Lake Oswego, OR, http://www.wavemetrics.com) and IVIS Living Image (Xenoxgen) software packages [14]. To detect photons from Luc$^+$ cells, undifferentiated MSCs or chondrocyte pellets were suspended in PBS and imaged immediately after the addition of 0.15 mg D-luciferin (potassium salt; Biosynth). Also, for transplanted cell tracking in vivo, D-luciferin was injected into the penile vein of anesthetized rats (30 mg/kg per body weight) under anesthesia with isoflurane. The signal intensity was quantified as photon flux in units of photons per seconds cm^2 per steradian in the region of interest.

Transmission Electron Microscopy

The regenerated tissues at 12 weeks in the synovium-MSCs treated group and control groups were selected and fixed with 2.5% glutaraldehyde in 0.1 M PBS for 5 hours, washed overnight at 4°C in the same buffer, postfixed with 1% OsO_4 buffered with 0.1 M PBS for 2 hours, dehydrated in a graded series of ethanol, and embedded in Epon 812. Ultrathin sections at 90 nm were collected on copper grids, double-stained with uranyl acetate and lead citrate, and then examined with a transmission electron microscope (H-7100, Hitachi, Hitachinaka, Japan, http://www.hitachi.co.jp) [15].

Quantitative Real-Time PCR

Total RNAs were prepared from brain, lung, liver, spleen, kidney, and knee synovium at 3 days after the synovium-MSCs injected rat by RNAqueous Kit (Ambion, ***Austin, TX***; http://www.ambion.com) according to the manufacturer's instructions. For the positive control, total RNAs from various organs of Luc/LacZ Tg rat and expanded MSCs including Luc/LacZ positive cell rates ranged from 0.001 to 100% were used. Also total RNAs from various organs of wild-type rat were prepared as a negative control. They were subjected to *real-time PCR* to measure the level of LacZ.

The primer sets for LacZ, (sense, 5′-GGTGCAGAGAGACAGGAACCAC-3′; antisense, 5′-CCTTCATACTGCACAGGTCTGCT-3′) and β-actin (sense, 5′-CCGAGCGTGGCTACAGCTT-3′; antisense, 5′-GGCAGTGGCCATCTCTTGC-3′) were synthesized at FASMAC (Kanagawa, Japan, http://www.fasmac.co.jp).

First-strand cDNA was synthesized using the I Script cDNA synthesis kit (Bio-Rad Laboratories, Hercules, CA, http://www.bio-rad.com) with an Oligo (dT) (12-18mers) primer. Real-time quantitative PCR analyses were performed with the ABI Prism 7700 Sequence Detection System (Applied Biosystems, Foster City, CA, http://www.appliedbiosystems.com) using SYBR Green I PCR reagents (TOYOBO, Osaka, Japan, http://www.toyobo.co.jp/e/) as described previously [12]. To determine the exact copy numbers of the target genes, the quantified concentrations of subcloned PCR fragments of LacZ and β-actin were serially diluted and used as standards in each experiment. Aliquots of cDNA equivalent to 5 ng of total RNA samples were used for each real-time PCR. Data were normalized with β-actin levels in each sample. The copy number is expressed as the number of transcripts per nanogram total RNA.

Statistics

The Mann-Whitney U test was used to compare two groups at each period. p values less than .05 were considered significant.

RESULTS

Synovium-MSCs Expressing Luc/LacZ Genes

The F1 hybrids between ROSA/luciferase Tg and ROSA/LacZ Lewis rat neonate produced luminescence after intraperitoneal injection of D-luciferin (Fig. 1A), and then they were positive for X-gal staining (Fig. 1B). In the same manner, we next examined luciferase and LacZ expression in various tissues of these rats. Approximately one-fourth of these F1 hybrids expressed luciferase and LacZ in whole body including the synovium (Fig. 1C). We termed these "dual colored" rats as Luc/LacZ Tg rats. MSCs were isolated from the synovium of Luc/LacZ Tg rats. In vitro imaging of luciferase activity showed that as few as one thousand MSCs were detected over the background in the linear dose-dependent output of luminescence (Fig. 1D, 1E). Synovium-MSCs from Luc/LacZ Tg rats formed LacZ$^+$ single cell-derived colonies consisting of spindle cells (Fig. 1F). They could differentiate into adipocytes (Fig. 1G) and calcified with LacZ expression in vitro (Fig. 1H). The cells could also form cartilage with expressions of both LacZ and luciferase (Fig. 1I). The cells derived from synovium of Luc/LacZ Tg rat demonstrated characteristics of MSCs, and the dual markers were maintained after the differentiation. Flow cytometric analysis demonstrated that the majority of synovium-MSCs expressed CD29 and CD90, and were negative for CD11b, CD34, and CD45 (Fig. 1J).

Hierarchical clustering analysis revealed that the gene expression of meniscal cells was closer to that of synovium-MSCs than that of bone marrow-MSCs (Fig. 2). This indicates that synovium-MSCs may retain a more advantageous character as a MSC source for meniscal regeneration than bone marrow-MSCs.

Meniscal Regeneration After Intra-articular Injection of Synovium-MSCs

To obtain in vivo evidence to support the synovium-MSCs potential, we performed massive meniscectomy in both sides

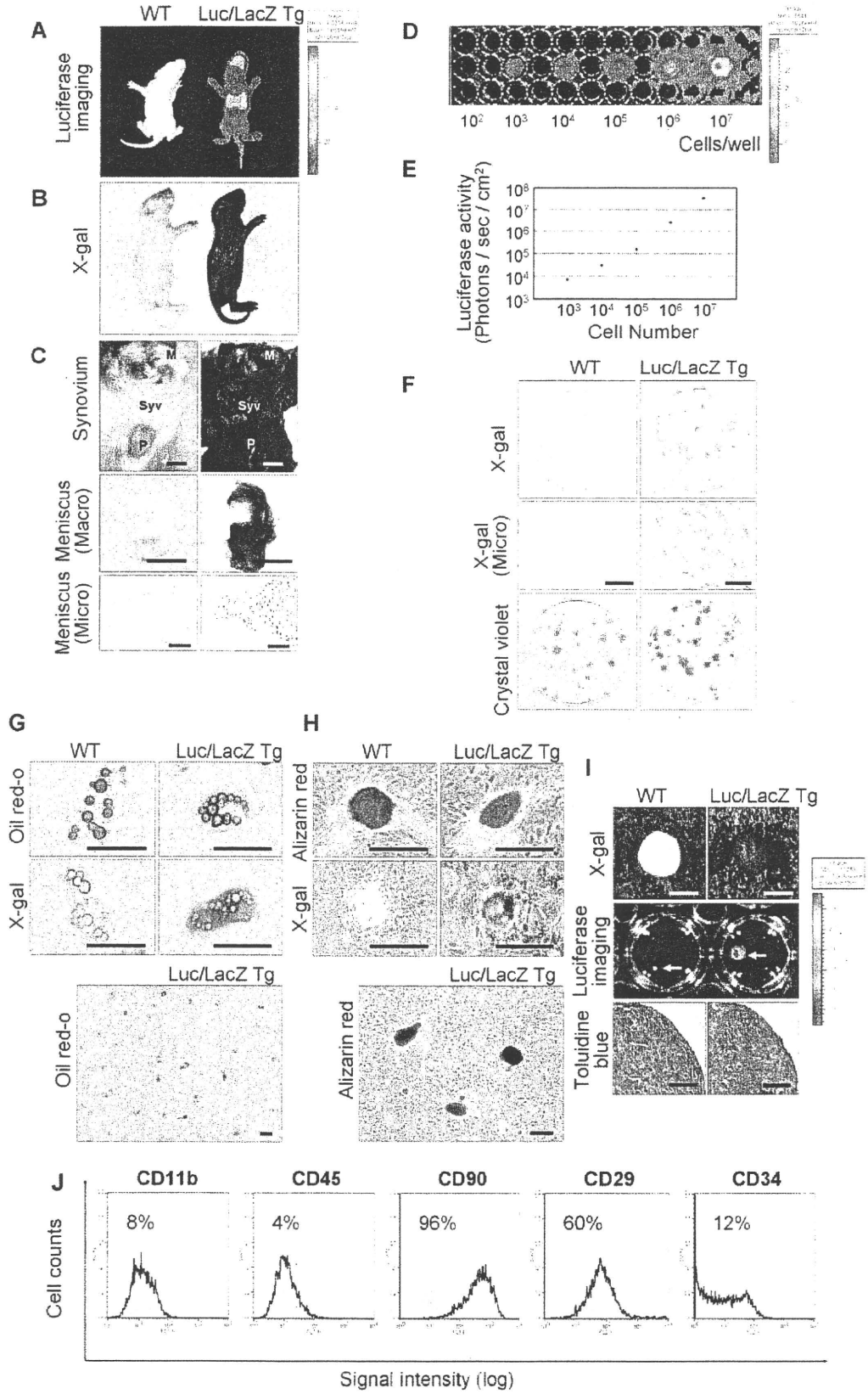

Figure 1. Mesenchymal stem cells (MSCs) derived from the synovium of Luc/LacZ transgenic (Tg) rats expressing dual reporter genes. **(A):** Luminescent images of wild and Luc/LacZ Tg rats. **(B):** Wild and Luc/LacZ Tg rats stained with X-gal. **(C):** Knee synovium and meniscus of wild and Luc/LacZ Tg rats stained with X-gal. Scale bar in upper and middle: 2 mm. Scale bar in lower: 100 μm. **(D):** Bioluminescent imaging of varying numbers of synovium-MSCs from Luc/LacZ Tg rats. **(E):** Quantification for bioluminescent imaging of varying numbers of synovium-MSCs. **(F):** Colony forming ability of MSCs from Luc/LacZ Tg rat synovium. X-gal positive colony forming cells 14 days after the plating of 100 cells in 60 cm^2 dishes (top). Microscopic appearances of X-gal positive spindle cells (middle). Scale bars: 50 μm. Total colonies in the same dishes stained with crystal violet (bottom). **(G):** Adipogenesis. Scale bars: 25 μm. **(H):** Calcification. Scale bars: 100 μm. **(I):** Chondrogenesis. Cartilage pellets stained with X-gal (top). Scale bars: 500 μm. Bioluminescent imaging of cartilage pellets (middle). Histological section stained with toluidine blue (bottom). Scale bar = 100 μm. **(J):** Flow cytometric analysis of synovium-MSCs at passage 3. CD11b, CD45, CD90, CD29, and CD 34 expression are shown as an open plot and isotype control expression as a shaded plot. Abbreviations: M, meniscus; P, patella; Syv, synovium; WT, wild-type.